Physics and Chemistry of the Earth 36 (2011) 1949–1959

Contents lists available at SciVerse ScienceDirect

Physics and Chemistry of the Earth

journal homepage: www.elsevier.com/locate/pce

Modeling the viscoplastic and damage behavior in deep argillaceous rocks

Mountaka Souley [a,*], Gilles Armand [b], Kun Su [c,1], Mehdi Ghoreychi [d]

[a] INERIS, Ecole des Mines, CS 14234, F-54042 Nancy Cedex, France
[b] ANDRA, Laboratoire souterrain de Meuse/Haute Marne, BP 9, 55290 Bure, France
[c] ANDRA, 1-7 rue Jean-Monnet, 92298 Châtenay-Malabry Cedex, France
[d] INERIS, Parc Technologique ALATA - BP 2, 60550 Verneuil-en-Halatte, France

ARTICLE INFO

Article history:
Available online 30 October 2011

Keywords:
Claystone
Laboratory characterization
In situ observations
Short and long terms behavior
Constitutive equations
Numercial implementation

ABSTRACT

In order to demonstrate the feasibility of a radioactive waste repository in the Callovo-Oxfordian claystone formation, the French national radioactive waste management agency (ANDRA) started in 2000 to build an underground research laboratory at Bure (East of France). One of the key issues is to understand long term behavior of the drifts.

More than 400 m horizontal galleries at the main level of −490 m have been instrumented since April 2005. The continuous measurements of convergence of the galleries are available, allowing a better understanding of the time-dependent response of the claystone at natural scale. Results indicate that the viscoplastic strain rates observed in the undamaged area far from the gallery walls are of the same order of magnitude as those obtained on rock samples, whereas those recorded in the damaged or fractured zone near the gallery walls are one to two orders of magnitude higher, indicating the significant influence of damage or/and macro-fractures on the viscoplastic strains.

Based on these observations, a macroscopic viscoplastic model which aims to improve the viscoplastic strain prediction in the EDZ is proposed and implemented in *FLAC*$^{3D©}$. Both the instantaneous and the time-dependent behavior are considered in the model. The short term response is assumed to be elacto-plastic with strain hardening/softening whereas the time-dependent behavior is based on the concepts of viscoplasticity (Lemaître's model). Finally, the damage-induced viscoplastic strains changes is examined through the plastic deformation (assumed to approach the damage rate).

In order to verify both constitutive equations and their implementations, several simulations are performed: (a) triaxial tests at different confining pressures; (b) single- and multi-stage creep tests; (c) relaxation tests with different total axial strain levels, etc. Finally, an example of a blind prediction of the excavation of a drift parallel to the horizontal minor stress, σ_h (gallery GED) is presented and compared to in situ measurements. The results show the influence of damage on viscoplastic strain rates and the advantages and disadvantages of this new approach are discussed.

1. Introduction

The excavation process creates a perturbed zone around underground structure openings in rock masses, where geotechnical and hydrogeological properties are altered. According to the degree of perturbation, this zone can be divided into two parts: the excavation disturbed zone (EdZ) and the excavation damaged zone (EDZ). The assessment of the disturbances in the rock mass surrounding deep galleries (EdZ or EDZ) due to the excavation, to pore pressure diffusion and to the gallery ventilation is quite important, especially in the context of nuclear wastes disposal in deep geological formations.

Between 1996 and 2004, in order to elaborate some mechanical and hydro-mechanical constitutive models, various campaigns of laboratory tests (uniaxial/triaxial, mono/multi stage creep and relaxation) have been undertaken to characterize the mechanical and hydro-mechanical short-term or long-term behavior of the claystone. Tests have been carried out on samples of the Callovo-Oxfordian argillite taken from the Meuse/Haute-Marne Underground Research Laboratory (MHM-URL). These programs consisted of more than 300 tests carried out by four different european laboratories. As a result, several constitutive models were developed in the framework of the MODEX-REP European project and of scientific cooperations between ANDRA and national research institutions (Su, 2003; ANDRA, 2005). For the short-term behavior, most of these models, developed within the framework of the plasticity theory and/or damage mechanics, are elastoplastic with strain hardening/softening and also account for damage. For the long-term

* Corresponding author.
E-mail address: mountaka.souley@ineris.fr (M. Souley).
[1] At present : Total, av. Larribau, 64018 Pau Cedex, France.

1474-7065/$ - see front matter
doi:10.1016/j.pce.2011.10.012

behavior, several teams agreed on adopting the modified Lemaître's model without or with creep threshold.

At the main level of the laboratory (−490 m), geo-mechanical measurements and the EDZ characterization have been performed (by monitoring convergence, using extensometers, etc.) in drifts either parallel or perpendicular to the horizontal major stress. Armand et al. (2009) describe the EDZ characterization and the induced fractures pattern observed during the excavation works. They show up that high deformation rates appear in the damaged and fractured area. The predictive calculations of these galleries intended to study the in situ time dependent behavior could not properly reproduce the observed deformations (Renaud et al., 2007).

In this paper, a new macroscopic elasto-plastic–viscoplastic model for the Callovo-Oxfordian claystone based on field observations and previous constitutive equations developed in the framework of the MODEX-REP program is presented. The model was developed in an attempt to improve the predictions of the viscoplastic strain around the drifts. The short term behavior is based on a previous work (Souley et al., 2003) where damage is approached through the theory of plasticity (even if the term "damage" refers to the initiation and the growth of micro-cracks). Consequently, the decrease of the elastic properties is not considered. In addition, the modeling of the long term behavior is based on an extension of the modified Lemaître's model. The changes in viscoplastic strain rates due to damage are taken into account by varying the creep activation energy and the strain-hardening as a function of the current damage (in terms of plastic deformations) rate.

The first opportunity to test the proposed model was to perform blind predictions of the behavior of gallery GCS parallel to the in situ majorhorizontal stress at the main level of MHM-URL, in the framework of a research program that started at the end of 2006. In this paper, the authors used the model, implemented in the *FLAC*$^{3D©}$ numerical code, to perform 3D calculations following the real construction steps of the gallery GED parallel to the minor horizontal in situ stress. Those calculations show up the advantage of the new model. Comparisons with in situ data allow checking the efficiency of this numerical approach.

2. Summary of laboratory characterization and first constitutive models

The initial water content of the samples ranged from 4.5% to 8.5%. Its role on the mechanical response of M/HM argillite has been demonstrated by laboratory tests (Zhang and Rothfuchs, 2004; Zhang et al., 2007). Since the permeability of the claystone is very low and since clay minerals are very sensitive to water content change, it is very difficult to carry out mechanical tests under the natural water content and pore pressure conditions without inducing additional damage of the material. Then, the tests were generally carried out with neither resaturation nor controlled pore water pressure.

The main features of the short-term mechanical behavior observed on the samples of claystone can be summarized as: (a) a linear behavior under low deviatoric stresses. In triaxial compression, the loss of linearity of stress-lateral strain curves begins approximately at 50% of the peak value of the deviatoric stress; (b) an appearance of plastic strains at low deviatoric stress; (c) under low confining pressures, the failure of the samples is brittle and corresponds to the formation of a shear band inclined with respect to the sample axis. There is a strong dependence of the mechanical behavior on the confining pressure, marked by a transition from a fragile towards a ductile behavior (Fig. 1). The post peak behavior as a function of the confining pressure has been captured with the external displacement sensors (Fig. 1b).

The experimental study of creep made it possible to characterize the long-term behavior with regard to the confining pressure, the mineralogical composition and the saturation level. The main features of the viscoplastic response can be summarized as follows: (a) the effect of the loading rate on the argillite strength is low and remains in the same order of magnitude as that resulting from the mineralogical variability; (b) the relaxation tests showed: (i) the stabilization of the deviatoric stress a few days after loading; (ii) the existence of a threshold below which the viscoplastic behavior is not activated; (c) simultaneous measurements of axial and lateral strains during creep tests show that volumetric strains are negligible; (d) during secondary creep in long-term tests, the creep strain rate increases in a non-linear way with applied deviatoric stresses ranging between 5 and 15 MPa. Moreover, creep strain rates slowly decrease with time. Finally, creep tests results show that the amplitude of the time-dependent deformations of the considered claystone was very small. The creep rate of core samples under undrained triaxial conditions ranges from about 10^{-6}–$10^{-7}\,h^{-1}$ (∼0.1% to 1% per year or 2.10^{-11}–$2.10^{-10}\,s^{-1}$) according to the loading rate and to the method used to assess the strain rate.

On the basis of these observations, several constitutive models for short-term as well as long-term behavior were developed for the Meuse/Haute-Marne claystone in the framework of the MODEX-REP European project (Su, 2003). For the short-term behavior, most of the models are elastoplastic with strain hardening/softening and they take into account damage through either the theory of plasticity or damage mechanics. Some of these models are hydro-mechanically coupled under saturated and/or unsaturated conditions. As a result, a constitutive model based on Hoek and Brown's criterion has been used by ANDRA for in situ experiment design purposes (Su, 2003; Souley et al., 2003).

For long-term behavior, several teams agree on the modified Lemaître's model without creep threshold. Certain authors (Miehe et al., 2003 in Su, 2003) proposed an elasto-viscoplastic model with instantaneous plasticity (say, a unification of both short-term and long-term behavior) without coupling the instantaneous plasticity and viscoplasticity. Consequently, the viscoplastic behavior in the post-failure range is exactly the same as that of the intact material and the failure criterion is not affected by the loading rate. This does not seem to be consistent with the high viscoplastic strain rates obtained in some creep tests under high deviatoric stresses close to failure or recently observed in situ in the vicinity of the MHM-URL drifts (see next section). In addition, in their works on the coupling between instantaneous plasticity and vicoplastic damage, Shao et al. (2003) or more recently Zhou et al. (2008) assume that the time-dependent degradation due the long-term behavior affects both the elastic modulus and the failure surface.

3. Data from in situ measurements: manifestations of damage/fracturing impact on the differed strains

During excavation, convergence measurements sections and radial extensometers have been implemented to follow the drift deformations. The following chapter depicts some of the typical measurements obtained in the drift at the main level of the MHM-URL.

A typical set-up installed in situ, mainly in the drifts parallel or perpendicular to the major horizontal stress presented by Wileveau et al. (2006) consists of (a) two instrumented arrays for convergence and displacement measurements set-up in place very close to the front face (around 1.5 m) in order to investigate deformation as a function of excavation steps and time (SUG1150, SUG1160, SUG1105, SUG1118); (b) arrays composed of radial extensometers, for which the end point, at 20 m far from the wall,

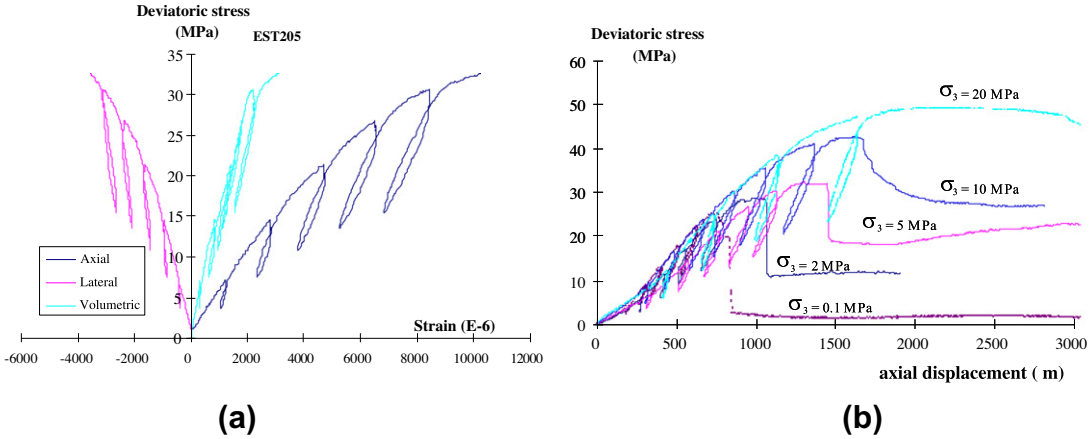

Fig. 1. Typical short-term response of East argillaceaous (a) triaxial stress–strains curves for a confining pressure of 5 MPa, (b) stress-displacement as a function of confining pressure (after Hoxha, 2005).

is considered as a fixed point and convergence sections (SUG1103, SUG1118, SUG1210).

The convergence of the drift has been measured at different locations during and after excavation. Some examples of measurements (vertical and horizontal) performed in different sections in the drifts parallel to σ_h are illustrated in Fig. 2. The vertical convergence exhibits enormous differences. After 3 years, the amplitude of the vertical convergence can change up to a ratio of 1.4. It is important to notice that sections SUG1150 and SUG1160 are one meter apart from each other. Horizontal convergences do not show such a heterogeneity.

Armand et al. (2009) presented the average evolution of convergence in drifts parallel or perpendicular to the major horizontal stress. Obviously, the behavior is very different in the two drift directions and it appears to be strongly linked to the in situ stress anisotropy. In the drifts parallel to σ_H, the evolutions of vertical and horizontal convergences are very similar. The horizontal convergence is slightly higher that the vertical one. The convergence rate, 3 years after the excavation, is 0.008 mm/day. In the drifts perpendicular to the horizontal major stress, the vertical convergence is much higher than the horizontal one. It could be noticed that the horizontal convergence measured in the drift parallel to σ_h is also smaller than that observed in the drift parallel to σ_H (nearly four times smaller). Three years after the excavation, the vertical convergence rate is 0.023 mm/day (three times higher than the convergence rate measured in a perpendicular drift).

The measurements also show that high convergence rates are related with the fracture extent. The description of the fracture pattern observed at the main level, with shear fractures (herringbone fractures and sub vertical fractures) and extension fractures can be found in Armand et al. (2007, 2009). The convergence amplitudes are in good agreement with the fracture extent. For example, in the drift parallel to σ_h, a significant convergence is observed between the floor and the vault where the fracture zone reaches nearly 2 m (plastic deformation).

The extensometers give the opportunity to better locate the high deformation rate in the vicinity of the drifts. Deformation has been calculated in between the different anchors of the vertical and horizontal extensometers at SMR1.1. Figs. 3 and 4 show the evolution of deformation as a function of time. The extensometer has been placed on 17th August 2005 at PM32.5. The excavation resumed on 19th August 2005 and was finalized on 28th September 2005, at PM49.6 (i.e. 17 m away from the extensometer section). The deformations increased a lot during the first 3 months (after the extensometer emplacement) even if the excavation work has been completed for 40 days. The most significant deformation

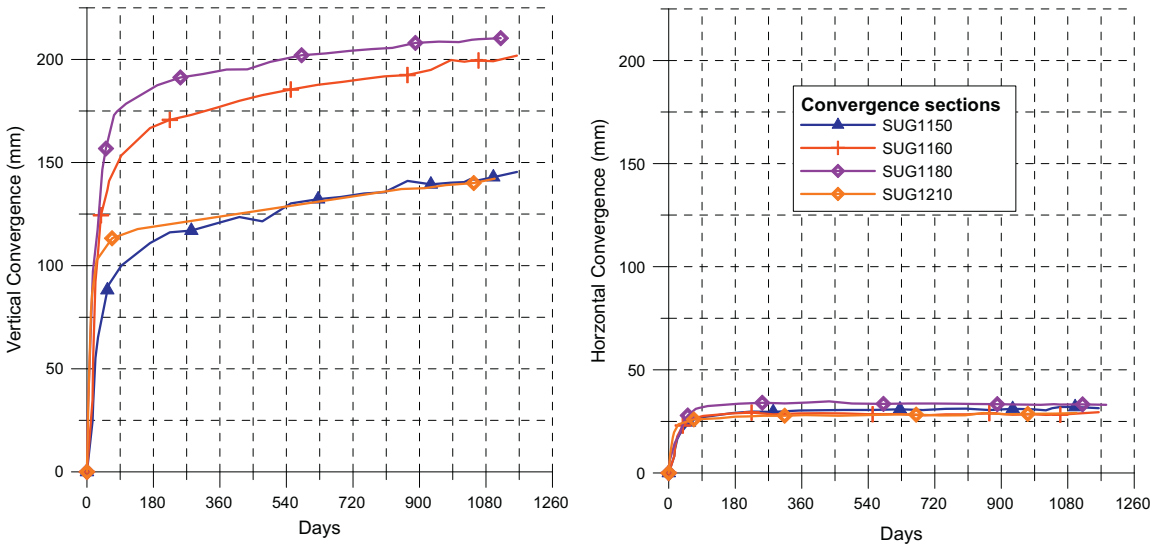

Fig. 2. Examples of vertical and horizontal convergences measured in drift parallel to σ_h.

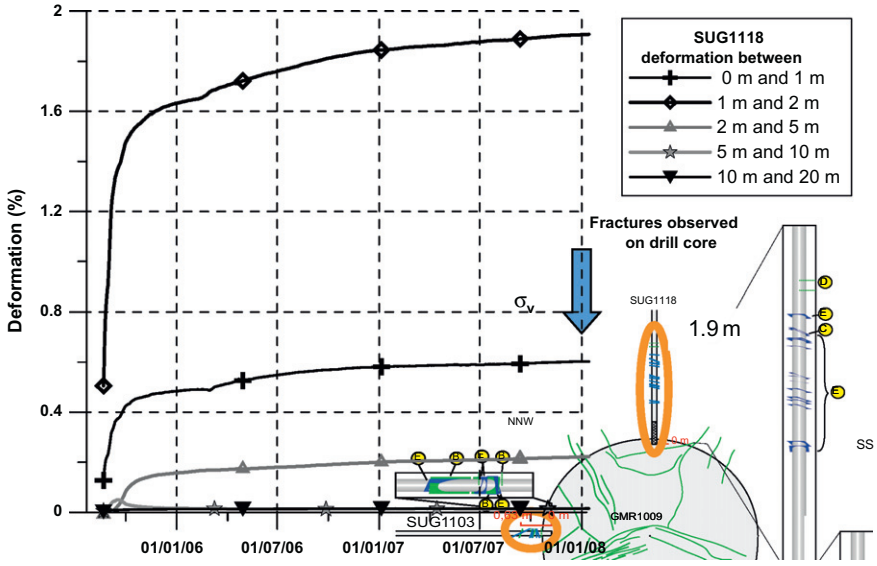

Fig. 3. Deformation measured in the vertical borehole (SUG1118) at the vault in the SMR1.1 (parallel to σ_h).

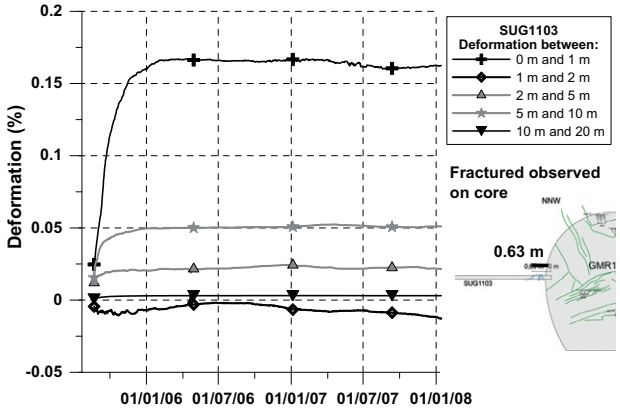

Fig. 4. Deformation measured in the horizontal borehole SUG1103 at the wall in the SMR1.1 (parallel to σ_h).

reaches nearly 2% and occurs between 1 and 2 m from the wall where the highest density of fractures has been observed by coring (Fig. 3). Between the wall and 1 m from the wall, the deformation remains significant.

On the horizontal extensometer (Fig. 4), the maximal deformation is less than 0.2% (10 times lower than the one measured at the vault). The higher deformation values are measured within the first meter from the wall where fractures have been observed on the drilled core. Between 1 m and 2 m from the wall, deformations are in compression since the beginning. This has to be explained (it could be an artefact due to the extensometer). Deformation measurements show that the highest deformation and deformation rate are localized in the fractures zone.

To conclude with in situ observations, the convergence and extensometer measurements suggest that the effect of the fractured zone on deformation is significant, meaning that the long term behavior of the rock mass is not representative of that of the fractured zone. All the observations carried out around the galleries of the MHM-URL at −490 m suggest a high influence of damage and fracturing on the time-dependent behavior of the galleries, through a significant increase of the time-dependent strains.

This observation led some authors (Renaud et al., 2007; Kleine, 2007) to propose a new parameters identification for the modified Lemaître's model, generally adopted to model the long-term behavior of claystone at natural scale on the basis of the previous convergence measurements. This makes it possible to reproduce some convergence measurements, but the application of these parameters to the whole rock mass or in the near field poses a problem, since the parameters were identified to measure the wall displacements where the damage rate is in principle maximum. The result above, shows the need to correctly evaluate the damaged and fractured zones at the natural scale and to correctly quantify the magnitude of deformation rates in these zones.

4. Proposed rheological model for both short and long terms behaviors

According to the experimental data obtained during the laboratory characterization and the in situ observations summarized in the previous sections, the mechanical behavior of Callovo-Oxfordian claystone is mainly dominated by plastic deformations in the short-term response and by time dependent deformations in the long-term response.

Firstly, the mechanical short-term behavior of agillites can be characterized by an elastoplastic approach. More precisely, the response of claystone to loading displays four phases describing the main aspects of the mechanical behavior (Fig. 1):

- phase I: linear elastic and isotropic behavior at low deviatoric stress;
- phase II: damage initiation and growth up to peak strength described by hardening plasticity. This concept is different from the concept of effective stress (Lemaitre, 1985) and the hypothesis of strain equivalence (Ju, 1989) that is generally used. Here, damage initiation and microcraks propagation are modeled by an elastoplastic model;
- phase III: post-peak (failure) associated with a progressive loss in material cohesion and a decrease in strength described by plasticity with softening;
- phase IV: residual phase where the rock strength remains practically constant for a given confining pressure.

The standard elastoplastic approach can be justified because of its simplicity and of the limited number of parameters (no damage variable) needed to easily model the experimental response of the

claystone. In addition, the use of hardening plasticity in the pre-peak region leads to estimate the extension of the micro-crack zone in the vicinity of the gallery. The macro-fractured zone corresponds to the domain where post failure has been reached (phases III and IV). By means of this approach of micro-crakings and macro-fractures in claystone, the extension of the plastic zone in the vicinity of a cavity can easily be estimated by numerical simulations.

However, for a more advanced modeling, it is useful to explicitly take into account the damage induced by micro-cracking, which is a significant dissipation mechanism since damage is higher when the confining pressure is very low. Then, an anisotropic damage induced by an oriented micro-crackings is developed as reported by Chiarelli et al. (2003) or Shao et al. (2006) when claystone are subjected to a desaturation process.

Secondly, it appears from creep tests (Su, 2003) that the long-term behavior is mainly characterized by the following features:

- creep strain rate accelerates non-linearly as deviatoric stress increases;
- creep strain rate varies as a function of viscoplastic strain; the analysis of this phenomenon suggests a strain-hardening function based on a power law;
- the trend of the creep strain rate to increase non-linearly with temperature may be expressed by an exponentially decreasing Arrhenius law;
- creep may take place beyond a creep threshold of 3 to 5 MPa. For practical applications, the deviatoric stress threshold can be chosen on the basis of the natural in situ stress state.

The following developments are based on the thermodynamics of continuous media with the assumption of small perturbations within a framework of isothermal elastoplasticity with strain-hardening/softening (for short-term response) and viscoplasticity (for long-term response). The state variables are: $\underline{\varepsilon}$ (total strain tensor); $\underline{\varepsilon}^p$ (time-independent instantaneous plastic strain tensor, including pre-peak damage and failure in post peak region); γ (accumulated plastic strain); $\underline{\varepsilon}^{vp}$ (time-dependent creep – or viscoplastic – strain tensor) and ε_{eq} (accumulated viscoplastic strain).

Assuming that only small strains occurred (as shown by the low strain rates measured in situ along a 2 years period as reported by Gasc-Barbier et al. (2004) and by the data from in situ investigations), the total strain can be expressed as the sum of the elastic strain $\underline{\varepsilon}^e$, of the instantaneous plastic strain and of the viscoplastic strain:

$$\underline{\varepsilon} = \underline{\varepsilon}^e + \underline{\varepsilon}^p + \underline{\varepsilon}^{vp} \tag{1}$$

Within the framework of the thermodynamics of irreversible processes, the free energy for an isotropic material can be subdivided into an elastic part, a plastic energy and a viscoplastic component as the following form:

$$\begin{aligned}\psi(\underline{\varepsilon},\underline{\varepsilon}^p,\gamma,\underline{\varepsilon}^{vp},\varepsilon_{eq}) &= \psi^e(\underline{\varepsilon}^e)+\psi^p(\underline{\varepsilon}^p,\gamma)+\psi^{vp}(\underline{\varepsilon}^{vp},\varepsilon_{eq})\\ &= \frac{1}{2}\underline{\varepsilon}^e : \underline{\underline{C}} : \underline{\varepsilon}^e + \psi^p(\underline{\varepsilon}^p,\gamma)+\psi^{vp}(\underline{\varepsilon}^{vp},\varepsilon_{eq})\\ &= \frac{1}{2}(\underline{\varepsilon}-\underline{\varepsilon}^p-\underline{\varepsilon}^{vp}) : \underline{\underline{C}} : (\underline{\varepsilon}-\underline{\varepsilon}^p-\underline{\varepsilon}^{vp})\\ &\quad + \psi^p(\underline{\varepsilon}^p,\gamma)+\psi^{vp}(\underline{\varepsilon}^{vp},\underline{\varepsilon}_{eq})\end{aligned} \tag{2}$$

$\psi$is the thermodynamic potential; ψ^e the thermoelastic potential; ψ^p the locked energy of the plastic flow and ψ^{vp} the viscoplastic component of the free energy.

The constitutive behavior is obtained by a standard derivation of the elastic potential with respect to the reversible elastic strain:

$$\sigma = \frac{\partial\psi^e(\underline{\varepsilon}^e)}{\partial\underline{\varepsilon}^e} = \frac{\partial\psi(\underline{\varepsilon},\underline{\varepsilon}^p,\gamma,\underline{\varepsilon}^{vp},\varepsilon_{eq})}{\partial\underline{\varepsilon}} = \underline{\underline{C}} : (\underline{\varepsilon}-\underline{\varepsilon}^p-\underline{\varepsilon}^{vp}) \tag{3}$$

where $\underline{\sigma}$ is the stress tensor.

The second principle of thermodynamics allows to write the Clausius–Duhem inequality, expressing the intrinsic dissipation d, according to the state variables and to the power of the internal forces by the stress tensor:

$$d = \underline{\sigma} : \dot{\underline{\varepsilon}} - \frac{\partial\psi}{\partial\alpha_k}\alpha_k \geqslant 0 \tag{4}$$

α_k represents the set of internal variable (scalar, vector or tensor).

It should be noted that the dissipation of the plastic strains in the claystone is mainly due to friction sliding of the clay minerals (Chiarelli et al., 2003). In the following, we will explicitly describe these state variables from the laboratory and in situ observations.

4.1. Case of instantaneous irreversible strains in pre and post peak

Based on the short-term experimental response obtained on the claystone samples, the plastic behavior (including damage in pre-peak and failure in post-peak) is approached by a modified Hoek–Brown yield function generalized in the space of the three stresses invariants. Moreover, the Hoek–Brown constants (m,s) and uniaxial compressive strength (σ_c) are used to define two independent internal variables A and B depending upon the equivalent plastic shear strain ($A = m\sigma_c$, $B = s\sigma_c^2$). The general form of the yield function (including the stress geometry through the Lode's angle, θ) is expressed in the following equation:

$$\begin{aligned}F_s(\underline{\sigma},\gamma) &= F_s(p,q,\theta,\gamma)\\ &= \frac{\left\{\frac{\chi(\gamma)}{\sigma_3^{b-d}}\left[p+q\left(\frac{\cos\theta}{\sqrt{3}}-\frac{\sin\theta}{3}\right)\right]-\frac{2}{\sqrt{3}}q\cos\theta+\chi(\gamma)\right\}^2}{A}\\ &\quad + p + q\left(\frac{\cos\theta}{\sqrt{3}}-\frac{\sin\theta}{3}\right)-\frac{B}{A}\end{aligned} \tag{5}$$

$$p = \frac{tr(\underline{\sigma})}{3} = \frac{\sigma_{kk}}{3}, q = \sqrt{3J_2}, \theta = \frac{1}{3}\sin^{-1}\left[-\frac{3\sqrt{3}}{2}\frac{J_3}{\sqrt{J_2^3}}\right] \tag{6}$$

$$J_2 = \frac{1}{2}\underline{s} : \underline{s}, J_3 = \det\underline{s}, \underline{s} = \underline{\sigma} - p\underline{I}$$

where p, q and θ are, respectively, the mean stress (compressive stresses are taken as negative), generalized deviatoric stress and Lode's angle. σ_3^{b-d} is the confining pressure leading to brittle/ductile transition and depending on the post-peak strength parameters. The parameter $\chi(\gamma)$ is the softening flow function parabolic form with respect to the internal plastic variable (equivalent plastic shear strain or plastic distortion) γ in phase III, and null elsewhere.

For simplicity, we assume here that A and B linearly vary with γ in phase II (from the onset of damage defined by: $m^{end}, s^{end}, \sigma_c^{end}$ to the peak defined by: $m^{rup}, s^{rup}, \sigma_c^{rup}$), and remain constant in phases III and IV.

In the literature, only few examples of implementation of the Hoek–Brown criterion in numerical codes are given and the existing implementations are generally based on rounding the corner and the apex, except the work of Clausen and Damkilde (2008). These authors developed an algorithm for the generalized Hoek–Brown criterion including the apex and corner singularities. The expression of the yield function given in Eq. (5) extends that initially proposed by Su (2003) or Souley et al. (2003). It proposes a regular form yield function allowing to be completely defined as well as its various derivatives in the all stress domain.

In their initial formulation, Souley et al. (2003) supposed an associated flow rule in claystone, for sake of simplicity. It is widely known that for most rock materials, a non-associated plastic flow rule is generally needed in order to reproduce the transition between plastic volumetric compressibility and dilatancy. In 2005, some complementary tests carried out on claystone samples made

it possible to specify the evolution of the irreversible volumetric deformation. From these tests, it came out that the hypothesis of associated flow rule tended to over-estimate the material dilatancy. Indeed, experimental data (Chiarelli et al., 2003; Zhang and Rothfuchs, 2004) exhibit a contractant behavior. At best, a dilatancy develops in the last phases of the tests according to the confining pressure.

This led us to assume herein a non-associated flow law and to propose the following plastic potential according to Drucker–Prager's criterion:

$$\Omega^p(\boldsymbol{\sigma},\gamma) = \eta(\gamma)p + q \tag{7}$$

$$\eta(\gamma) = \frac{2\sqrt{3}\sin[\psi(\gamma)]}{(3+\sin[\psi(\gamma)])} \tag{8}$$

where ψ represents the dilatancy angle, the values of which, obtained by laboratory tests, vary between the onset of damage (ψ^{end}), the peak (ψ^{rup}) and the beginning of residual phase (ψ^{res}). We assume that ψ varies linearly with respect to the internal variable γ and remains constant ($\psi = \psi^{res}$) while the residual strength is reached (say a bilinear relation from the onset of damage to the start of residual phase).

The damaged/plastic strain increment is given by:

$$d\underline{\varepsilon}^p = \lambda\frac{\partial\Omega^p}{\partial\underline{\sigma}} \tag{9}$$

$$d\gamma = \lambda\frac{\partial\Omega^p}{\partial q} = \sqrt{\frac{2}{3}d\underline{e}^p : d\underline{e}^p} = \sqrt{\frac{2}{3}de^p_{ij}de^p_{ij}} \text{ with } d\underline{e}^p = d\underline{\varepsilon}^p - \frac{tr(d\underline{\varepsilon}^p)}{3}\underline{I} \tag{10}$$

where λ is the plastic multiplier determined from the consistency condition $dF_s(\underline{\sigma},\gamma) = 0$.

4.2. Case of time-dependent irreversible strains (viscoplastic strains)

The understanding of the long-term behavior is of primary importance, especially for repository design and reversibility. Consequently, it is useful to consider that the time-dependent behavior of material is related to the deformation processes corresponding to different physical mechanisms of microstructure modification of the material. By using the well-known formalism proposed by Perzyna (1966), it is possible to express the total viscoplastic strain rate:

$$\dot{\underline{\varepsilon}}^{vp} = \frac{1}{\eta}\langle\Phi(f^{vp})\rangle\frac{\partial g^{vp}}{\partial\underline{\sigma}} \tag{11}$$

where η is the viscosity coefficient, f^{vp} the loading function for the viscoplastic mechanism (viscoplastic criterion), g^{vp} the viscoplastic flow potential, $\langle\ \rangle$ the MacCauley function. According to the overstress concept proposed by Perzyna (1966), the positive values of $\langle\Phi\ (f^{vp})\rangle$ define the distance between the current stress state and the corresponding loading surface.

More precisely, based on the main observations from creep tests, a creep model is proposed (Su, 2003) by introducing a creep threshold function in the well-known Lemaitre's law. By taking all the observed phenomena (detailed in the beginning of this section) into account, the following expression was proposed for the viscoplastic strain rate tensor:

$$\dot{\underline{\varepsilon}}^{vp} = A_0(T)\exp\left(-\frac{B}{RT}\right)\left(\frac{q-q_0}{\sigma_0}\right)^n(\varepsilon_{eq})^m\frac{\partial q}{\partial\underline{\sigma}} \tag{12}$$

where B is the activation energy, R the Boltzmann constant; T the absolute temperature, A_0 the intact material viscosity at a reference temperature, σ_0 the reference stress, n a dimensionless exponent corresponding to the deviatoric stress power factor, m the exponent of hardening work, $\varepsilon_{eq} = \sqrt{\frac{2}{3}\underline{\varepsilon}^{vp} : \underline{\varepsilon}^{vp}}$ the viscoplastic strain (or viscoplastic distortion in accordance with the observed negligible volumetric strains during creep tests). q_0 is the deviatoric stress threshold, that can be generalized to a creep threshold function depending on the natural in situ stress state (p_0,q_0) and on the difference between the natural stress state and the induced ones (p,q) for practical applications.

In situ observations highlighted the influence of damage on the creep strain rate. In the same way, when the deviatoric stress reaches a certain value between 15 and 18 MPa, creep tests also showed that Lemaître's model (with its parameters identified from the tests with stress level lower than 15 MPa) under-estimated the strains. These observations lead us to express the influence of damage on the viscoplastic strain rate through one or several following forms: (a) the exponent n of the deviatoric stress; (b) the activation energy; (c) the hardening power factor. Since the deviatoric stress is rather related to the loading history (its increase making the damage growth) and in order to reduce the number of input parameters and their identification, we firstly preferred to vary the hardening exponent and the activation energy with respect to the damage state. Moreover, it was supposed that in the post-failure range the material would have some creep characteristics which differ from those of the intact material. In particular the viscoplastic strain rate and the activation energy must reflect the failure of the claystone.

Let m_0 and $m_1 (0 > m_0 \geqslant m_1)$ be the hardening parameter corresponding to the intact (undamaged) and post-failure materials, respectively. In lack of experimental data (i.e. abscence of creep tests on different damaged samples of claystone), we propose an evolution of parameter m between m_0 and m_1 which supposes low slopes near the two extreme states (undamaged and broken):

$$m = m(\gamma) = 2(m_0-m_1)(\gamma^*)^3 - 3(m_0-m_1)(\gamma^*)^2 + m_0 \tag{13}$$

$\gamma^* = \min(\gamma/\gamma^{rup},1)$: where γ and γ^{rup} are the current and peak value of the plastic shear strain.

By postulating that the influence of damage on the creep activation energy can be approached by an exponential function: $\exp(b_1\gamma^*)$, the viscoplastic strain rate is expressed as follows:

$$\dot{\underline{\varepsilon}}^{vp} = A_0(T)\exp\left(-\frac{B}{RT}+b_1\gamma^*\right)\left(\frac{q-q_0}{\sigma_0}\right)^n(\varepsilon_{eq})^{m(\gamma^*)}\frac{\partial q}{\partial\underline{\sigma}} \tag{14}$$

The extension of the long-term behavior taking into account the damage rate of claystone samples presented in this paper is based on the following main assumptions:

(1) the fractured zone observed around the drifts of the main level of the MHM-URL is supposed to be continuous so as to use the mechanics of continuous media, in a purpose of simplification;
(2) when the material reaches the peak strength, it is considered to be completely broken with some constant viscoplastic characteristics. Certainly in the reality, the start and the end of the post peak phase are characterized by a difference of the sample damage rate and probably there exists a transition between a domain corresponding to a few grown micro-cracks (beginning of the post-peak phase) and that of the macro-fractures near the residual. This is the case of the conceptual model proposed by Kolmayer et al. (2004). In their model, the beginning of the post-peak domain corresponds to the deterioration of the rock's cementation, with a progressively disappearing cohesion. This mechanism is followed by a phase governed by the growth of micro-cracks towards the heart of material and by a residual phase corresponding to a purely frictional state. By assuming this

concept in the post-peak regime, it would be necessary to be able to perform several creep tests (very difficult to operate) according to the various material states in post-peak domain in order to approach the progressive evolution of the microstructure.

It should be noticed that the coupling between the induced damage and the creep behavior is only clarified in one way: (damage → viscoplastic strain rates) since we did not consider up to now the influence of viscoplastic strains on the damage threshold (as proposed by Zhou et al., 2008). Also, viscoplastic strains modify the stress field that, in turn, is corrected while it exceeds the damage criterion, possibly changing the EDZ extent. Moreover, without an available data, the influence of viscosity on the long-term strength of the claystone is not taken into account in the model, even though if the induced damage may be responsible for the material failure and for the strength decreases when the loading rate decreases.

Finally, the consistency condition $dF_s(\underline{\underline{\sigma}},\gamma)=0$ allows to express the stress increment as a function of total and viscoplastic strain increments through the fourth order elastic compliance tensor $\underline{\underline{C}}$:

$$d\underline{\underline{\sigma}}=\left[\underline{\underline{C}}-\frac{\left(\underline{\underline{C}}:\frac{\partial F_s}{\partial\underline{\underline{\sigma}}}\right)\otimes\left(\underline{\underline{C}}:\frac{\partial\Omega^p}{\partial\underline{\underline{\sigma}}}\right)}{\frac{\partial F_s}{\partial\underline{\underline{\sigma}}}:\underline{\underline{C}}:\frac{\partial\Omega^p}{\partial\underline{\underline{\sigma}}}-\frac{\partial F_s}{\partial\gamma}\frac{\Omega^p}{\partial q}}\right]:(d\underline{\underline{\varepsilon}}-d\underline{\underline{\varepsilon}}^{vp}) \quad (15)$$

Except for constants m_1 and b_1, all parameters have already been identified either from creep tests on intact material, or from triaxial tests for the short-term response (Su, 2003). Since only the results of two creep tests with deviatoric stress close to the peak value (say on damaged materials) are available, the constants m_1 and b_1 are back-evaluated from the observed in situ convergences (Souley et al., 2009).

5. Numerical implementation, verification and validation

5.1. Numerical implementation

The model was implemented by coupling the damage state with the viscoplastic strain rate as described above in the three-dimensional explicit finite-difference code, *FLAC*$^{3D©}$. At each creep time-step, Eqs. (14) and (15) are solved using the Crank-Nicolson method and a central-difference formulation (Fig. 5).

5.2. Verification and validation

In order to verify the short-term part of the model, seven triaxial compression tests with confining pressures of 2, 5, 10, 12, 16, 20 and 25 MPa are simulated (they are a part of the wide number of triaxial compression tests characterizing the non-linear behavior of the studied materials). The resulting curves (not presented in this paper) display four regions (elastic, damage in pre-peak, softening in post-peak and residual phases) when the confining pressure is below the transition stress level σ_3^{b-d}. It displays three regions (elastic, damage and perfect plastic phase) under high confining pressure. In addition, the onset of damage (limit between elastic/damage region), the peak and the residual strengths derived from these simulations have been compared with the theoretical envelopes, showing that the corresponding relative error did not exceed 0.3%.

5.2.1. Short term behavior: associated flow rule versus non associated flow rule

In this section, we examine the assumption of a non associated flow rule by comparing with the initial associated model (Souley et al., 2003) and a laboratory compression test under a 5 MPa confining pressure (Figs. 6 and 7). The simulation was performed firstly by assuming ψ values of 0°, 15° and 30° at the onset of damage (ψ^{end}), at peak (ψ^{rup}) and at the beginning of residual phase (ψ^{res}), respectively. In the second simulation, the dilatancy only occurs in the post peak regime ($\psi^{end}=\psi^{rup}=0°$, $\psi^{res}=15°$). The proposed model satisfactory reproduces the mechanical behavior of the argillite, including the main phases of damage, failure and post failure. The non associated plastic flow rule correctly describes the volumetric strain measured before failure. In the post failure phase, the proposed continuous model cannot reproduce the volumetric deformation at low confining pressure when the shear displacement of strips controls the mechanical response.

5.2.2. Long term behavior: validation on relaxation tests perfromed under moderate deviatoric stress

The model is now applied to simulate some relaxation tests performed on claystone under a confining pressure of 10 MPa, presented in Su (2003). The evolutions of deviatoric stress with time for the four tests are recalled in Fig. 8. The numerical simulation carried out with the model is also shown in Fig. 8. Since the deviatoric stress reached before relaxation is lower than the onset of damage (approximately 20 MPa for 10 MPa of confining pressure), the sample remains undamaged. Qualitatively, the model response is in good agreement with the experimental curves. From a quantitative point of view, the model is perfectly in agreement with the results of test E5083_7 and E5171_4 for the rate of stress relaxation at the beginning of test. In addition, both observed and predicted deviatoric stress reach the same plateau at the end of test.

5.2.3. Long term behavior: validation on relaxation tests perfromed under moderate deviatoric stress

Fig. 9 shows the effect of damage on the viscoplastic strains obtained from the simulations of triaxial multi-level creep tests under a confining pressure of about 10 MPa. In the first simulation (without effect of damage), it was assumed that both the undamaged and broken materials behaved similarly ($m_1=m_0$; $b_1=0$). At the first stage, since the onset of damage is not reached, the evolution of the viscoplastic distortion remains identical. The two last stages correspond to two different levels of material damage: 30% and 70% of maximum damage prior to failure (peak). It should be noticed that when the damage rate is high, the viscoplastic strains become increasingly large.

6. Application to GED drift

6.1. Experimental layout of GED drift

The drift network of the MHM-URL has been axcavated following both horizontal principal stresses. The GED drift is located far away from the other drifts and was excavated with a pneumatic hammer, perpendicular to the horizontal major stress (Fig. 10). The supports consist of 2.2 m radial bolts, 10 cm of synthetic fibers reinforced shotcrete and sliding steel arches installed every meter. The front was also reinforced with 11 synthetic anchors (12 m long) placed every 6 m. Excavation started in May 2008 and was finalized by the end of January 2009.

The experiment layout consists of six convergence sections, with five convergence measurements per section, four 30 meters long extensometers (with seven measurements anchors at 1, 2, 3.5, 5, 8, 15 and 30 m from the wall) and four 1 m long extensometers. A geological mapping of the front was made every 5 m and the structural analysis of all cored boreholes (even in borehole performed for other experiments) has been carried out during the excavation to properly characterize the fracture zone. Extensometer and convergence sections have been installed during excavation. The other boreholes will be drilled after the excavation.

✓ Compute the old deviatoric stress tensor: $\underline{s}^{old} = \underline{\sigma}^{old} - \frac{1}{3} tr\left(\underline{\sigma}^{old}\right)\underline{\delta}$

✓ For it=1, Nmax (Crank-Nicholson explicit sheme)

If it=1

$\underline{s}^{m} = \underline{s}^{old}$

$\varepsilon_{eq}^{\ m} = \varepsilon_{eq}^{\ old}$

Else

$\underline{s}^{m} = \left(\underline{s}^{m} + \underline{s}^{old}\right)/2$

$\varepsilon_{eq}^{\ m} = \left(\varepsilon_{eq}^{\ n} + \varepsilon_{eq}^{\ old}\right)/2$

Endif

} Central difference to compute the mean deviatoric stress tensor and viscoplastic strain

Compute the Von Mises stress: $q = \sqrt{\frac{3}{2}\underline{s}^{m} : \underline{s}^{m}}$

Compute the viscoplastic strain rate: Eq. (14)

Compute the viscoplastic strain tensor increment: $d\underline{\varepsilon}^{vp} = \frac{3}{2}\dot{\varepsilon}_{eq}\frac{\underline{s}^{m}}{q}\Delta t$

Compute the instantaneous strain tensor increment: $d\underline{\varepsilon}^{inst} = d\underline{\varepsilon}^{e} + d\underline{\varepsilon}^{p} = d\underline{\varepsilon} - d\underline{\varepsilon}^{vp}$

Based on the total instantaneous strain increment, compute the new stresses (elastoplasticity): $\underline{\sigma}^{n}$

$\underline{s}^{n} = \underline{\sigma}^{n} - \frac{1}{3} tr\left(\underline{\sigma}^{n}\right)\underline{\delta}$

$\varepsilon_{eq}^{\ n} = \varepsilon_{eq}^{\ old} + \dot{\varepsilon}_{eq}\Delta t$

✓ Update internal (damage, plastic and viscoplastic) variables

Fig. 5. A simplified flowchart of the proposed model.

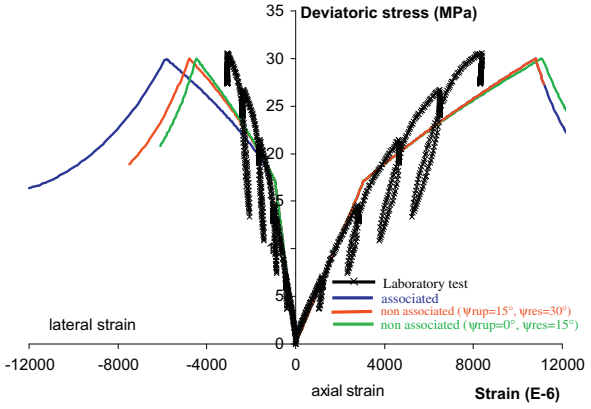

Fig. 6. Comparison with the axial and lateral stress–strain curves: axial and lateral strains.

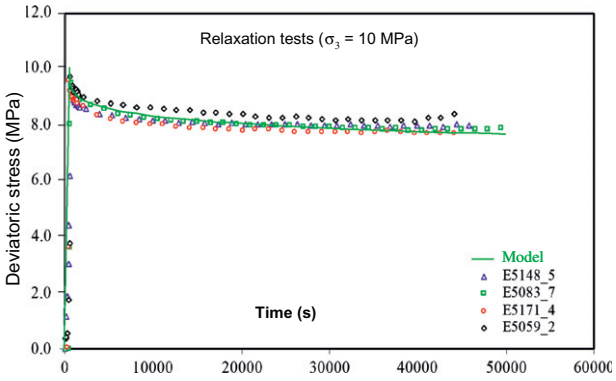

Fig. 8. Simulation of relaxation test using the proposed model: comparison with the laboratory tests.

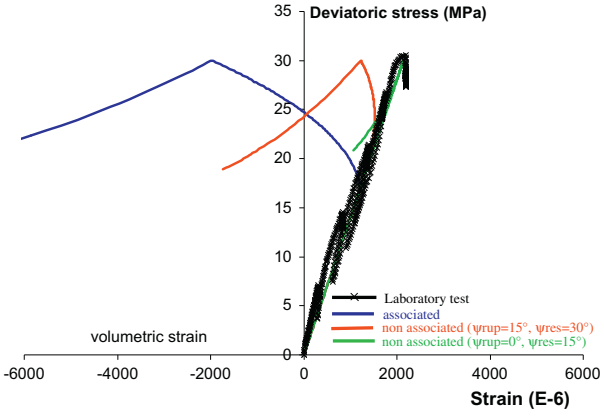

Fig. 7. Comparison with axial and lateral stress–strain curves: volumetric strain.

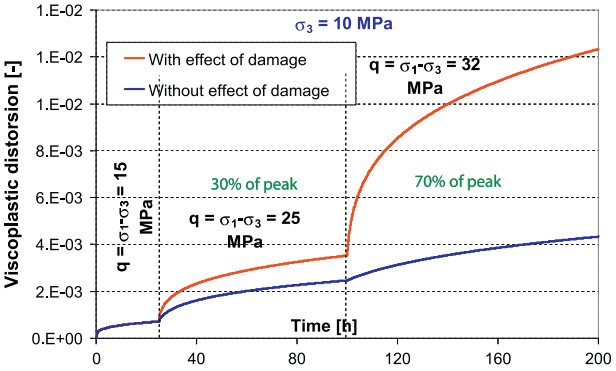

Fig. 9. Viscoplastic shear strain for a multi-stage creep test simulation (1st stage q = 15 MPa; 2nd stage q = 25 MPa and 3rd stage q = 32 MPa).

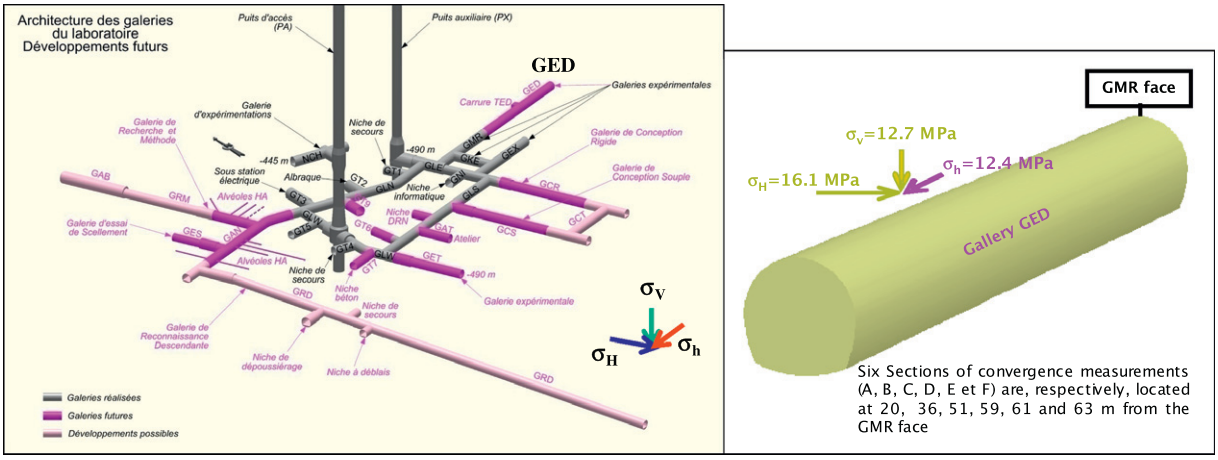

Fig. 10. Drifts shaft network (purple: extension forecasted in 2012). (For interpretation of the references to colour in this figure legend, the reader is referred to the web version of this article.)

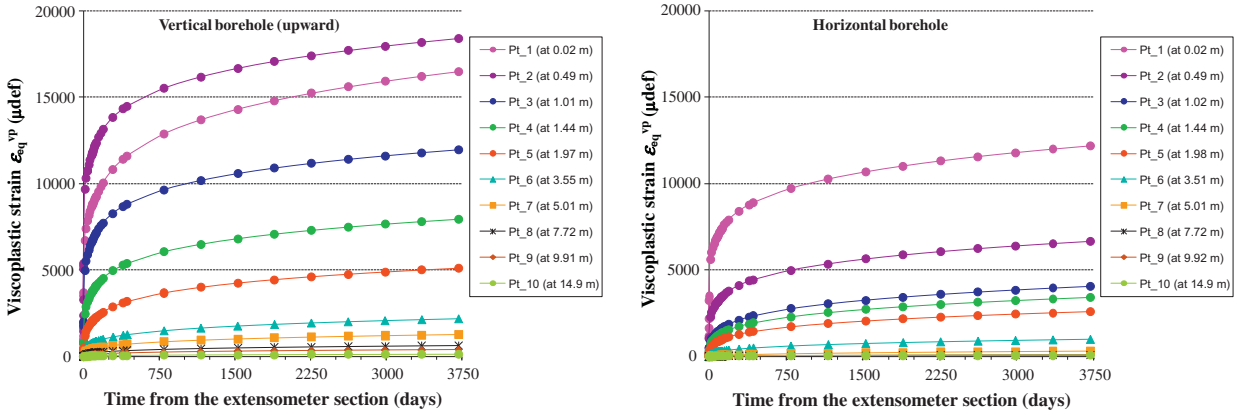

Fig. 11. Viscoplastic strains along vertical and horizontal boreholes (section C).

Multi-packer systems with 3 or 6 chambers from the wall to 6 m deep have also been placed to perform pore pressure measurements and permeability tests. The corresponding data are not presented here because the numerical analysis is only mechanical.

The in situ stress state at the Meuse/Haute-Marne site has been measured by comprehensive combined methods (Wileveau et al., 2007) and the vertical stress profile is presently well-known. The horizontal stress anisotropy σ_H/σ_h is close to 1.3 close at the main level (−490 m), with σ_H and σ_h respectively equal to 12.7 and 12.4 MPa.

6.2. Numerical modeling

In relation to the symmetry of GED drift (70 m long and considered as isolated) and its orientation with respect to the initial stress state (parallel to σ_h), only the half domain is modeled. The geometrical model (150 m high, 57 m wide and 100 m long) consists of 574,770 elements with the following characteristics. The meshing consists of 5 cm radially around the measurement sections A, B, C, D, E and F (respectively located at 19.5, 35.5, 51.5, 59, 61 and 63.5 m from the beginning of GED drift) and 40 cm axially on both sides of each measurement section. The real advance velocity of 1 m/day (except during the break time to install the equipments) during the drilling of GED is used.

The EDZ distribution around the GED drift is firstly examined from numerical simulation. When the face is positioned at sections B and C for example, the fractured zones (from peak to residual behavior) are not yet formed around the drift. From a face at 5 m after each section (i.e. two gallery radii) to the end of excavation, the fractured zones extend from 0 to 29 cm depending on the position (floor, roof of drift side) and on the section.

Contrary, a damaged zone (pre-peak behavior) is systematically formed as soon as the GED face reaches the position of a given section (80, 110 and 120 cm, respectively at side, roof and floor of GED). In relation to the anisotropy of the in situ stress state, more damage is obtained in the vertical direction compared to the horizontal ones (along σ_H) whereas the slight difference in EDZ geometry and extent between the floor and the roof is related to their geometries. The extent of the damaged zone becomes 170, 260 and 270 cm, respectively at side, roof and floor at the end of excavation.

The evolutions of the viscoplastic strains with time are also investigated along vertical and horizontal boreholes in section C (Fig. 11). If the maximum of deformation in the horizontal direction is reached at the GED sides, the model predicts a maximum viscoplastic strain inside the rock matrix in the vertical directions. It is also observed that the amplitude of the viscoplastic deformations is well correlated to the intensity and extension of the EDZ (i.e. high viscoplastic strains occur in the more damaged zones), in accordance with the philosophy of the model and the in situ observations. In particular, at the end of 10 years, the predicted viscoplastic strain rates at 2 m from the GED wall of $2e^{-12}$ and $4e^{-12}$ s^{-1} in the horizontal and vertical directions, respectively.

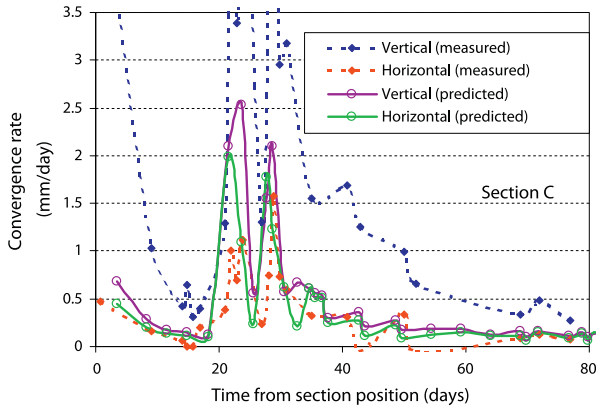

Fig. 12. Comparison of calculated and measured convergence rates.

6.3. Comparison with in situ measurements

The analysis of the measured and predicted convergences shows that in the vertical direction and independently of the measurements section: (a) the short-term velocity of the measured convergences are higher than those predicted whereas in the long-term, we can expect that the measured convergence velocities tend asymptotically towards the predictions; (b) the amplitudes of measured convergences are higher than those predicted (Fig. 12). In particular, calculation under-estimates from 13% to 44% the vertical convergence respectively in sections B and C at the end of 80 days.

For horizontal convergences, we note that at 80 days after the passage of GED face through a given section, the measured/predicted convergences are 23/30 mm and 33/27 mm and 18/39 mm for sections A, B and C, respectively. This illustrates the over-estimation of the calculations in the horizontal direction.

7. Conclusion

This paper presented the development of a model for the long-term behavior of the Callovo-Oxfordian claystone. The model integrates the deformations measured in the laboratory and corresponding to that observed in situ. The impact of the damaged and fractured zones in the near field close to the cavities on the amplitude of the viscoplastic deformations is also considered in a simplified and pragmatic manner, using plastic strain (approaching the damage rate) and activation energy.

The model is developed from experimental considerations, based on laboratory characterization as well as in situ evidences of damage influence on viscoplastic strains. More precisely, it generalizes two rheological models developed in the framework of the MODEX-REP European project: one for the short-term response (in which damage is approached by using the plasticity theory and the criterion of Hoek–Brown), the other for the long-term behavior (according to the modified Lemaître's model).

The changes of viscoplastic strain rates due to damage are taken into account by varying the creep activation energy and the strain-hardening as a function of the current damage rate.

The proposed macroscopic model is implemented in the three-dimensional code *FLAC*$^{3D©}$. Simulations of triaxial compression tests under different confining pressures provide a verification of the implemented model, in particular by comparing the predicted damage threshold, peak and residual strengths profiles with the theoretical ones.

The simulation of laboratory relaxation tests allows to confirm that the proposed model is relevant since the input parameters for the time-dependent behavior are derived only from creep tests. The model prediction is in agreement with the measurements and the results of Shao et al. (2003).

Finally, this paper also presented a 3D blind prediction of the behavior of a GED drift oriented parallel to σ_h. The comparison of the convergence predictions in six sections and the first measurements indicates that the model under-estimates the values of vertical convergences and over-estimates horizontal convergences. On the other hand, the convergences rates are well produced particularly in the horizontal direction during 100 first days after excavation. Further developments of the model, particularly for the fractured zones (viscoplastic rates and modules), will be considered. They will integrate the convergence and extensometer measurements currently in acquisition, as well as some confrontation with the futur results of the Mine-by test of the gallery GCS oriented parallel to the maximum horizontal principal stress.

Appendix A. List of parameters and input values

Parameter	Unit	Input value	Significance
Short term behavior			
E	(MPa)	4000	Young's modulus
ν	(–)	0.3	Poisson's coefficient
σ_c^{end}	(MPa)	9.6	Uniaxial compressive strength corresponding to the elastic limit
m^{end}, s^{end}	(–)	1.5, 1	Hoek and Brown constants at the onset of damage (limit of elastic limit)
σ_c^{rup}	(MPa)	33.5	Uniaxial compressive strength (at peak)
m^{rup}, s^{rup}	(–)	2, 0.128	Hoek and Brown constants at the peak
α	(–)	2.8	Parameter associated the transition between brittle and ductile failure
β	(MPa)	3	Resdual strength without confining pressure
ψ^{end}, ψ^{rup}, ψ^{res}	(°)	0, 15, 30	Dilatancy angle respectively at the onset of damage, the peak and the residual phase
γ^{rup}, γ^{res}	(–)	0.00575, 0.0155	Plastic distorsion at the peak and the beginning of residual phase
Long term behavior			
A_0	h^{-1}	4.17 10^{-11}	Intact material viscosity at a reference temperature
n	(–)	6.8	Dimensionless exponent traducing the deviatoric stress power factor in the Lemaitre model
m_0	(–)	−2.7	Exponent of hardening work for intact material
m_1	(–)	−5.75	Exponent of hardening work for failed material (post peak and residual phases)
b	(–)	1.6	Parameter relating the damage (in pre-peak) influence on the activation energy

References

ANDRA, 2005. Référentiel du site de Meuse/Haute-Marne – tome 2 - volume 5. Andra report no C.RP.ADS.04.0022, December. <www.andra.fr>

Armand, G., Nussbaum, C., Cruchaudet, M., Rebours, H., 2009. Characterisation of the Excavated Damaged Zone (EDZ) in the Meuse Haute-Marne underground research laboratory. In: Proceedings of the International Conference on Rock Joints and Jointed Rock Masses. January 4–9, Tucson, USA

Armand, G., Wileveau, Y., Morel, J., Cruchaudet, M., Rebours, H., 2007. Excavated Damaged Zone (EDZ) in the Meuse Haute-Marne underground research laboratory. In: Ribeiro e Sousa, L. (Ed.), Proceedings of the 11th Congress of the ISRM, 9–13 July. Lisbon, Portugal, pp. 33–36.

Chiarelli, A.S., Shao, J.F., Hoteit, N., 2003. Modelling of elastic-plastic damage behaviour of a claystone. Int. J. Plast. 19, 23–45.

Clausen, J., Damkilde, L., 2008. An exact implementation of the Hoek–Brown criterion for elasto-plastic finite element calculations. Int. J. Rock Mech. Min. Sci. 45 (6), 831–847.

Gasc-Barbier, M., Chanchole, S., Bérest, P., 2004. Creep behaviour of Bure clayey rock. Appl. Clay Sci. 26 (20), 449–458.

Hoxha, D., 2005. Modélisation des géomatériaux. Mémoire d'Habilitation à Diriger des Recherches de l'INPL, 79p. + annexe

Ju, JW., 1989. On the energy based on coupled elastoplastic damage theories: constitutive modeling and computational aspects. Int. J. Solids Struct. 25 (7), 803–833.

Kleine, A., 2007. Modélisation numérique du comportement des ouvrages souterrains par une approche viscoplastique. Thèse de Doctorat de l'INPL, 301p. + annexes

Kolmayer, P., Fernandes, R., Chavant, C., 2004. Numerical implementation of a new rheological law for argilites. Appl. Clay Sci. 26, 499–510.

Lemaitre, J., 1985. A Course on Damage Mechanics, second ed. Springer.

Perzyna, P., 1966. Fundamental problems in viscoplasticity. Adv. Appl. Mech. 9, 243–377.

Renaud, V., Maison, T., Wileveau, Y., Armand, G., 2007. Various approaches for the comprehension of the time dependant behavior of Callovo-Oxfordian argillites. In: International Meeting "Clays in Natural and Engineered Barriers for Radioactive Wasteconfinement", 9-12 September. Lille.

Shao, J.F., Jia, Y., Kondo, D., Chiarelli, A.S., 2006. A coupled elastoplastic damage model for semi-brittle materials and extension to unsaturated conditions. Mech. Mater. 38, 218–232.

Shao, J.F., Zhu, Q.Z., Su, K., 2003. Modeling of creep in rock materials in terms of material degradation. Comput. Geotech. 30, 549–555.

Souley, M., Su, K., Ghoreychi, M., Armand, G., 2003. Constitutive models for rock mass: numerical implementation, verification and validation. In: Brummer et al. (Eds.), FLAC and Numerical Modeling in Geomech. ISBN 90 5809 581 9.

Souley, M., Su, K., Ghoreychi, M., Armand, G., 2009. A viscoplastic model including damage for deep argillaceous rocks. In: 1st International Symposium on Computational Geomechanics (ComGeo I), April 29–May 1st. Juan-les-Pins, Cote d'Azur, France.

Su, K., 2003. Constitutive Models for the Meuse/Haute-Marne Argillites – MODEX-REP, European Commission – Nuclear science and technology, Contract n° FIKW-CT2000-00029, Deliverable 2-3

Wileveau, Y., Cornet, F.H., Desroches, J., Blumling, P., 2007. Complete in situ stress determination in an argillite sedimentary formation. Phys. Chem. Earth 32, 866–878.

Wileveau, Y., Renaud, V., Kazmierczak, J.-B., Armand, G., 2006. Rheological characterization of a clay formation from drifts excavation: elastic and elastoplastic approach. In: Proceedings of Sea to Sky Geotechnique. Vancouver, Canada, p. 006.

Zhang, C-L., Rothfuchs, T., Su, K., Hoteit, N., 2007. Experimental Study of the thermo-hydro-mechanical Behavior of Indurated Clays. Part 2. Phys. Chem. Earth 32 (8–14), 957–965.

Zhang, C.L., Rothfuchs, T., 2004. Experimental study of the hydromechanical behaviour of the Callovo-Oxfordian argillite. Appl. Clay Sci. 26, 325–336.

Zhou, H., Jia, Y., Shao, J.F., 2008. A unified elastic–plastic and viscoplastic damage model for quasi-brittle rocks. Int. J. Rock. Mech. Min. Sci. 45 (8), 1237–1251.